miR-206 Enforces a Slow Muscle Phenotype

Kristen K. Bjorkman[1], Martin G. Guess[1], Brooke C. Harrison[1], Michael M. Polmear[1], Angela K. Peter[1], Leslie A. Leinwand[1,2]

1. Department of Molecular, Cellular, and Developmental Biology

BioFrontiers Institute

University of Colorado Boulder

3415 Colorado Ave.

UCB596

Boulder, CO USA 80303

2. To whom correspondence should be addressed: leslie.leinwand@colorado.edu

Abstract

Striated muscle is a highly specialized collection of tissues that have different contractile properties depending on their functional roles. These properties derive from differential gene expression, including sarcomeric genes such as myosin heavy chains (MyHCs) and metabolic genes that coordinate energy demands with the contractile machinery. Although muscle fiber types are established shortly after birth, there is lifelong plasticity that facilitates adaptation to both physiologic and pathologic stimuli. Functional adaptation requires molecular adaptation, and this is partially provided by miRNA-mediated post-transcriptional regulation. Several miRNAs are specific to muscle, including miR-206, which is particularly associated with slow oxidative muscles and is up-regulated in conditions that shift fast muscles towards a slower phenotype. We sought to determine whether miR-206 is a driver of the slow muscle phenotype or merely a terminal outcome. We found that miR-206 expression increases in both physiologic

(female sex and endurance exercise) and pathologic conditions (muscular dystrophy and response to acute injury) that promote the slow phenotype. We also found that the predominantly slow soleus displays a faster phenotype in miR-206 knockout mice. Left ventricles of these animals also have a faster MyHC profile that is accompanied by dilation and systolic dysfunction. Interestingly, these phenotypes were male-specific. Our data indicate that miR-206 is necessary to enforce the slow straited muscle phenotype and that miR-206 plays a key role in sexual dimorphisms in cardiac and skeletal muscle.

Introduction

Skeletal muscle is a highly organized contractile tissue that composes 40% of human body mass (Janssen et al., 2000). Muscle subgroups are further specialized to perform a diverse array of functions, such as chewing, moving and focusing the eye, breathing, maintaining body posture, and both burst and sustained movements. To meet these various demands, different muscle types are characterized by different metabolic and contractile machinery. Oxidative myofibers are more fatigue-resistant and have higher mitochondrial content to facilitate β-oxidation. They can be further subdivided into slow oxidative and fast oxidative myofibers. Slow oxidative fibers are also called type I fibers due to expression of type I/β-myosin heavy chain (MyHC), a member of the sarcomeric MyHC protein family which ultimately confers contractile properties on the muscle. Fast oxidative fibers express type IIa, IIx, or a mixture of those two faster MyHCs. They also are more oxidative than type I fibers, presumably to accommodate the greater ATP demands of types IIa and IIx MyHCs compared to type I (Chemello et al., 2019). Fast glycolytic myofibers fatigue more easily and rely on glycolysis for energy production. They express the fastest MyHC, type IIb or a IIx/IIb mixture, to promote higher contraction speed.

Although fiber types are established shortly after birth (Gokhin et al., 2008), adult skeletal muscle retains remarkable plasticity in order to adapt to changing demands. In addition to tuning performance, muscle is a metabolically demanding tissue that is critical to maintaining homeostasis body-wide due to the balance of energy substrate utilization. Physiological stimuli such as short sprint versus endurance exercise training shifts muscles to a more glycolytic or more oxidative phenotype, respectively (Allen et al., 2001; Andersen and Henriksson, 1977; Ross and Leveritt, 2001). Muscle unloading due to a variety of stimuli typically results in a more glycolytic profile (Caiozzo et al., 1998; Harrison et al., 2003; McCarthy et al., 1997). Certain pathologic states, including muscular dystrophy, result in a shift to more oxidative/slow fibers in part because fast fibers are more susceptible to damage (Webster et al., 1988). Finally, although understudied, evidence from rodents to humans suggests that many female muscles are slower than their male counterparts (Haizlip et al., 2015; Janssen et al., 2000).

Cardiomyocytes, the contractile cells in cardiac muscle, express two MyHCs in mammals: the same β-MyHC found in Type I skeletal muscle fibers as well as the faster, cardiac-restricted α-MyHC. There is also evidence that female cardiac muscle is slower than male (Patrizio et al., 2013; Trexler et al., 2017). While most mammalian species express both MyHCs, the α:β ratio varies between species but is tightly controlled within a species. Mice typically express >99% α-MyHC while humans express >90% β (Izumo et al., 1987; Miyata et al., 2000). However, β-MyHC levels increase in most types of heart disease, regardless of species (Miyata et al., 2000; Nakao et al., 1997). This is presumably a compensatory response as the slower, more energetically efficient β-MyHC may be more suited to the metabolic stress that typifies many forms of heart disease. However, the accompanying reduction in contractility ultimately renders this a maladaptive long-term response.

Tuning the gene expression profiles in these fiber types occurs through a coordinated transcriptional and post-transcriptional network. miRNA-mediated post-transcriptional regulation is a key event in muscle development: Skeletal muscle-specific knockout of Dicer, which prevents all miRNA maturation in this tissue, is embryonic lethal (O'Rourke et al., 2007). Several miRNAs have been specifically shown to modulate muscle fiber type. For example, double knockout of the two miR-133a genes doubles the percentage of type I fibers at the expense of type II fibers in the soleus, suggesting it enforces a fast program (Liu et al., 2011). In addition, miR-27a promotes a fast oxidative (type IIa) phenotype while miR-499 and miR-208b promote the type I phenotype (Chemello et al., 2019; van Rooij et al., 2009). Along with the miR-208/499 and miR-133 family, the miR-1/206 family is also predominantly expressed in muscle (Ma et al., 2015; McCarthy, 2008; Mitchelson, 2015). In the basal state, miR-206 is most highly enriched in slow muscle (Boettger et al., 2014; Williams et al., 2009). miR-206 is also up-regulated in fast muscle in several pathologic settings, including the chronic, progressive damage associated with amyotrophic lateral sclerosis (ALS) and Duchenne muscular dystrophy (DMD) as well as acute chemical injury from cardiotoxin injection (Liu et al., 2012; Williams et al., 2009; Yuasa et al., 2008). In conditions associated with mixed fiber type muscle shifting towards a faster profile such as spaceflight and aging, miR-206 levels decrease (Allen et al., 2009; Hamrick et al., 2010; Kim et al., 2014). Notably, despite a general sex difference in muscle fiber types, it is not known whether biological sex influences miR-206 expression. Thus, we sought to determine in both sexes whether the miR-206 slow muscle enrichment is an outcome or a driver of the oxidative phenotype.

Materials and Methods

Cloning and mutagenesis: The minimal promoter (minTATA) and MyoG enhancer firefly luciferase reporter gene consructs were previously described (Cheung et al., 2007). We cloned the miR-206 enhancer (GRCm38/mm10 chr1:20,678,053-20,678,259) in the same manner as described for MyoG. We generated E-box point mutations (CANNTG → CANNTA) with the Quikchange II site-directed mutagenesis kit (Stratagene) per the manufacturer's instructions. MRF expression constructs were a kind gift from Dr. Xuedong Liu (University of Colorado Boulder). Primer sequences are listed in Supplemental Table 1.

Cell culture and transfection: We grew C2C12 myoblasts in Growth Medium (GM): high glucose DMEM (Invitrogen 11960069) supplemented with 20% fetal bovine serum, 2 mM L-glutamine, 100 U/mL penicillin and 100 μg/mL streptomycin, and 1 mM sodium pyruvate. We differentiated them to myotubes by changing media to Differentiation Medium (DM): high glucose DMEM supplemented with 5% adult horse serum, 2 mM L-glutamine, 100 U/mL penicillin and 100 μg/mL streptomycin, and 1 mM sodium pyruvate. When differentiating, we refreshed DM every day to prevent media acidification. We grew 10T ½ cells in GM but with 10% FBS. For luciferase assays, we plated cells in triplicate in 6-well dishes at a density of 50,000 cells/well (C2C12) or 100,000 cells/well (10T ½) 24 hours before transfection. We transfected with *Trans*IT-LT1 (Mirus, MIR 2305) according to the manufacturer's instructions. We co-transfected all firefly luciferase constructs with pRL-TK as a control. When differentiating C2C12 myotubes, we collected Day 0 timepoints 24 hours post-transfection and initiated differentiation at the same time for later timepoints. We collected 10T1/2 cells 24 hours post-transfection. At harvest, we washed cells twice with phosphate-buffered saline (PBS) solution and stored them in an ultralow freezer in order to process all timepoints together at the end of the experiment.

Luciferase assays: We used a Dual-Luciferase Reporter Assay System (Promega, E1960) according to the manufacturer's instructions with a Turner Designs TD-20/20 luminometer. Briefly, we lysed frozen cells in 1X Passive Lysis Buffer and measured reporter gene activities first in LARII reagent (firefly luciferase) and second in Stop & Glo reagent (Renilla luciferase). Read times for both were 10 seconds. We compared Renilla/firefly ratios.

Mice: All wild-type C57Bl/6, miR-206 KO (a kind gift from Dr. Eric Olson, University of Texas Southwestern Medical Center and described in (Williams et al., 2009)), and *mdx4cv* were between 4 and 7 months old. Aromatase knockout (ArKO) mice were 4 months old as this age precedes the age-dependent increase in testosterone observed in the ArKO females (Haines et al., 2012). Mice were housed in standard temperature and humidity-controlled environments with a 12-hour light-dark cycle and offered food and water *ad libidum*. We euthanized mice by cervical dislocation under inhaled isoflurane. We excised and flash froze in liquid nitrogen all tissues used for molecular analyses. For muscles used for sectioning and staining, we excised and embedded in OCT compound and then froze them in melting isopentane chilled with liquid nitrogen. The University of Colorado Boulder and Colorado State University Institutional Animal Care and Use Committees approved all animal work.

Cage Activity: To model endurance exercise, we provided a cage wheel to mice and allowed them to run voluntarily as previously described (Allen et al., 2001). To model muscle unloading, we performed hindlimb suspension as previously described (Allen et al., 2009). We suspended the tail at a 30° angle by taping it to a plastic dowel attached to a swivel apparatus. The forelimbs were still in contact with the cage bottom. We attached the suspension apparatus to a guide wire so mice were able to access all areas of the cage. We euthanized mice and harvested tissues 3, 7,

or 14 days after initiating exercise or hindlimb suspension. We compared samples from exercised or hindlimb suspension mice to age-matched normal cage activity controls.

Isoproterenol treatment: We chronically administered isoproterenol in 1μM ascorbic acid diluted in sterile saline to C57Bl/6J wild-type male mice (Jackson Laboratories, 000664, Sarcramento, CA) via subcutaneous implantation of a miniosmotic pump (model 2001; Alzet, Cupertino, CA). The pumps delivered isoproterenol at a dose of 30 or 45 mg/kg body weight per day. Vehicle control pumps contained 1μM ascorbic acid diluted in sterile saline . We euthanized mice as described above seven days after pump implantation.

$BaCl_2$ injury: We injured the TA or gastrocnemius with barium chloride as previously described (Guess et al., 2013). Briefly, we anesthetized wild-type male mice with 1-4% inhaled isoflurane and shaved the right hind limb. We cleaned the shaved area with 70% ethanol and used a 27-gauge insulin syringe to inject the right gastrocnemius with 50 μL of 1.2% $BaCl_2$ dissolved in normal saline. We monitored mice for adverse effects while they recovered on a 37C heat block.

Echo: We performed M-mode echocardiographic measurements as previously described (Haines et al., 2012). Heart rate was the same in all groups (Supp. Fig. 7A).

Hydrodynamic limb vein injection and *in vivo* imaging: We performed hydrodynamic limb vein (HLV) injections and subsequent *in vivo* reporter gene activity imaging as previously described in (Guess et al., 2013). Briefly, we co-injected the miR-206 enhancer-driven luciferase plasmid or the basal promoter-only (minTATA) control plasmid with the normalization construct p-mKate, which expresses a far red fluorescent protein from a constitutively active promoter.

Human biopsies: Human DMD (kindly provided by Dr. Eric Hoffman of George Washington University) and healthy control vastus lateralis (VL) biopsy samples were previously described

(Guess et al., 2015). The University of Colorado Human Research Institutional Review Board (IRB) considered the DMD samples exempt from approval according to the University of Colorado Human Research IRB guidelines and approved collection of control biopsies under IRB Protocol 0402.11, August 2002.

Sectioning and immunostaining: We cut 10 μm sections from the mid-belly of the soleus and immunostained with standard techniques. For fiber typing, primary antibodies against different MyHC isoforms were all from Developmental Studies Hybridoma Bank (MyHC IIa (SC-71), MyHC IIx (6H1), and β-MyHC (BA-D5)). We used isotype-specific secondary antibodies (FITC-goat α-mouse IgM (Jackson 115-095-075), AlexaFluor568-goat α-mouse IgG1 (Invitrogen A-21124), and AlexaFluor647-goat α-mouse IgG2b (Jackson 15-605-207)). For cross-sectional area calculations, we delineated individual myofibers with α-laminin (Sigma L-9393) staining and FITC-donkey α-rabbit (Jackson 711-095-152) as secondary. We stained DNA with DAPI. We collected all images on a Nikon TE2000 inverted fluorescent microscope with a 20X objective connected to a Nikon DS-QiMc-U3 camera controlled through the NIS-Elements AR software version 4.00.03. We kept exposure times for a given channel constant for all slides. We processed raw images with the Image5D plugin in ImageJ using the same settings for a given channel across all images.

Fiber typing: In ImageJ, we manually counted fiber types across entire soleus sections based on MyHC immunostaining. This analysis was double blinded.

CSA measurements: We manually measured myofiber cross-sectional area across entire laminin-stained soleus sections using ImageJ. This analysis was also double-blinded.

RNA isolation and qPCR analysis: We isolated total RNA with TRI Reagent (MRC TR 118) according to the manufacturer's protocol. We homogenized tissue samples directly into TRI reagent using a dispersion tool (IKA T10 Basic S1). For pri-miR-206 analysis, we DNase treated the RNA (TURBO DNA-free kit; Thermo Fisher AM1907) as the qPCR primers could not be intron-spanning. We performed all qPCR on an ABI 7500 Fast Real-Time PCR System. We assessed miRNA expression by TaqMan-based qPCR (ThermoFisher, Part Number 4427975). We reverse transcribed miRNAs with a TaqMan MicroRNA Reverse Transcription Kit (ThermoFisher, 4366596) and performed qPCR with TaqMan Universal PCR Master Mix, No AmpErase UNG (ThermoFisher, 4324018), all according to the manufacturer's instructions. We used the $\Delta\Delta C_T$ method to analyze relative expression. We normalized all mouse miRNAs to sno202 expression levels and human miR-206 to U6 RNA. We measured mRNA expression with SYBR Green-based qPCR. All primer sequences are listed in Supplemental Table 1. We reverse transcribed total RNA with random hexamer primers using the Superscript II Reverse Transcriptase kit (ThermoFisher, 18064-022). We performed qPCR with SYBR Green PCR Master Mix (ThermoFisher, 4312704) according to the manufacturer's instructions. We measured relative expression with the Pfaffl standard curve method. In regenerating TA (Fig. 2D), we normalized pri-miR-206 levels to 18S rRNA. In 206KO and WT soleus (Fig. 5), we normalized mRNA levels to Acta1, and in the heart (Fig. 6 and Supplemental Fig. 8), we normalized mRNA levels to Gapdh.

Graphing and Statistical analysis: We graphed and analyzed all data for statistical significance with GraphPad Prism. We analyzed simple two-group comparisons with a Student's t-test. We analyzed multi-group comparisons with ANOVA followed by a Bonferroni post-test. We chose a

p-value of 0.05 as the significance threshold. Other cutoffs are as noted in the figure legends. Data are presented as means with error bars representing standard error of the mean.

Results

<u>miR-206 is associated with a slow-twitch muscle phenotype but is higher in fast female muscles.</u> We measured miR-206 levels in three mouse lower hindlimb muscles with different fiber type compositions. In both males and females, we found a stepwise increase in miR-206 expression from the fastest muscle (tibialis anterior (TA)) to a mixed fiber type muscle (gastrocnemius and plantaris (GP)) to the slowest muscle (soleus (SOL)). Fig 1A reveals approximately 30-fold enrichment in soleus compared to TA. Interestingly, we measured significantly higher miR-206 levels in female TA compared to male (Fig. 1A, right panel), which correlates with our previous observation that the female TA contains a greater fraction of slow fibers than the male TA (Haizlip et al., 2015). There was no sex difference in the expression of the other myomiRs (miR-1, miR-133b, or miR-133a) in the TA (Supp. Fig. 1A). Since miR-206 levels can differentially respond to liganding of different estrogen receptors in breast cancer cells (Adams et al., 2007), we assessed a potential hormonal basis for the sex difference in the TA by examining miR-206 levels in female aromatase knockout (ArKO) mice, which do not produce any estrogen. In ArKO TA, we observed a significant 1.3-fold reduction in miR-206 levels (Fig. 1B), while miRs -1, -133b, and -133a were unaffected (Supp. Fig. 1C) , suggesting a miR-206-specific phenomenon. There was no change in the ArKO GP and a downward trend of similar magnitude in the ArKO soleus (p = 0.052; Supp. Fig. 1B). As it is well known that endurance exercise induces a shift towards a slow twitch phenotype (Allen et al., 2001; Andersen and Henriksson, 1977), we examined miR-206 expression in the TAs of male WT mice running voluntarily on exercise wheels. miR-206 levels increased 5.3-fold after 3 days of exercise and returned to sedentary

levels by 7 days, remaining there at 14 days (Fig. 1C). Hindlimb suspension, a model of muscle disuse that can induce a fast-twitch shift, did not result in changes in miR-206 expression (Fig. 1C).

We next evaluated whether miR-206 expression responds to pathologic muscle stimuli that shift typical fast muscles to a slower phenotype. One characteristic of Duchenne muscular dystrophy (DMD) is selective sparing of slow muscle and disproportionate loss of fast muscle (Webster et al., 1988). In addition, the damage-induced regeneration in the earlier phases of the disease is accompanied by re-expression of embryonic myosin heavy chain (MyHC), one of the slowest sarcomeric myosins (Ciciliot and Schiaffino, 2010; Resnicow et al., 2010). In agreement with both of these observations, in the *mdx4cv* mouse model of DMD we saw miR-206 induced in both TA and GP with no change in the soleus (Fig. 2A). We confirmed this induction in human DMD vastus lateralis biopsies, a normally mixed fiber type thigh muscle (Fig. 2B). Muscle regeneration in response to acute injury also includes a transient period of slow embryonic MyHC re-expression before re-establishing the normal adult muscle phenotype. Accordingly, we found a stepwise increase in miR-206 expression during a two week regeneration time course in $BaCl_2$-injured TA (Fig. 2C). This increase is due to transcriptional activation as we observed a robust induction of the primary miR-206 transcript that preceded peak levels of the mature miRNA and then decreased towards basal levels as regeneration proceeded (Fig. 2D). We further corroborated this transcriptional induction *in vivo* by injecting a luciferase reporter gene controlled by a 200-bp upstream miR-206 enhancer (Supp. Fig. 3A) into GP that we subsequently injured with $BaCl_2$. During the regeneration time course we saw a peak in luciferase activity three days post-injury, consistent with the peak in endogenous pri-miR-206 levels (Fig. 2E). This behavior was dependent on the miR-206 enhancer as there was no injury

response from a construct with just a basal promoter driving luciferase (Fig. 2E and Supp. Fig. 2). As previously reported, we also saw that this enhancer region responded to endogenous myogenic cues in differentiating C2C12 mouse myoblasts and in 10T1/2 mouse fibroblasts transfected with each of the four muscle regulatory factors (MyoD, myogenin, MRF4, Myf5; Supp. Fig. 3B,C). MyoD is known to bind this region (Rao et al., 2006; Sweetman et al., 2008), and there are five E-boxes with the generic consensus CANNTG (Supp. Fig. 3A). A more refined muscle consensus site has been proposed that has a more specific core hexamer (CA(C/G)(C/G)TG) and extended flanking sequence (Yutzey and Konieczny, 1992). We found that the 1st, 2nd, and 5th E-boxes conform well to this muscle consensus but the 3rd and 4th do not (Supp. Fig. 3D). In agreement, only the muscle consensus E-boxes are conserved in the human genome and mutation of only these E-boxes abolished the reporter response to C2C12 differentiation (Supp. Fig. 3E). Moreover, a reporter construct with the orthologous human enhancer also responds to mouse C2C12 differentiation cues (data not shown). This region has also been reported to function as a transcriptional enhancer dependent on the same E-boxes in neonatal rat cardiomyocytes (Yang et al., 2015).

<u>miR-206 deletion results in a slow-to-fast muscle switch.</u> We next investigated whether miR-206 expression is an outcome or a driver of the slow muscle phenotype by examining the miR-206 knockout mouse (206KO) (Williams et al., 2009). We found a male-specific increase in soleus weight while the faster TA and GP muscles were unaffected (Fig. 3A and Supp. Fig. 4). Histological examination of 206KO soleus cross-sections suggested there were larger fibers than in wild-type counterparts (representative images Fig. 3B). Indeed, we observed an enrichment for larger fibers and a depletion of small fibers in 206KO soleus when we measured cross-sectional area (Fig. 3C). This effect is specific to lack of miR-206 as we did not observe any

compensatory change in the closely related miR-1 nor any perturbation in the genetically linked miR-133b (Supp. Fig. 5A) or in linc-MD1, the non-coding RNA also generated from this locus (Supp. Fig. 5B). We further characterized the phenotype of the 206KO soleus through MyHC fiber typing. We stained cross-sections with antibodies specific to slow type I (β-MyHC), intermediate type IIa, and fast type IIx (representative images Fig. 4A). Relative to wild-type, we calculated a 25% decrease in the proportion of type I fibers and a 14% increase in the proportion of type IIa fibers in 206KO mice. Type IIx fibers are rare in the predominantly slow soleus, but we observed a striking increase in the fraction of these fast fibers in 206KO mice. While this was not statistically significant due to inter-animal variability, it is noteworthy (Fig. 4B). Corroborating these fiber typing data, we saw a modest change in β-MyHC mRNA but a significant 2.5-fold increase in MyHC IIa. Again we measured the largest increase (3.4-fold) in MyHC IIx mRNA (Fig. 4C). MyHC IIb was essentially undetectable in the soleus of either genotype (data not shown).

To extend our molecular profiling of 206KO soleus, we measured expression levels of RNAs typically enriched in either slow or fast skeletal muscle (Fig. 5). We considered transcription factors, non-coding RNAs, troponin isoforms, and metabolic factors in addition to the MyHC signature described above. Amongst transcription factors, we found a two-fold up-regulation of the slow-associated Mef2c as well as the fast-associated Six1 and Eya1. While at first this may seem contradictory, we address this more fully in the Discussion below. We found no change in the slow-associated miRNAs miR-208b and miR-499 but a two-fold up-regulation of the fast-associated long non-coding RNA linc-MYH. Beyond the MyHC complement, contractile properties are also tuned by functionally distinct isoforms of other sarcomere components, including troponins. In skeletal muscle, the Tnni2 isoform of troponin I is fast-

associated while Tnni1 is slow-associated. We did not see changes in the expression of either isoform. Expression of the slow-associated calcium-handling factor Serca2a did not change and there was a modest but significant increase in the oxygen-binding protein myoglobin (Mb). When we consider these data in conjunction with the MyHC analysis, we see an overall shift towards inducing a fast oxidative muscle phenotype in the absence of miR-206, indicating it is likely to be an enforcer of the slow program.

<u>miR-206 deletion results in cardiac dilation.</u> In a healthy rodent heart, miR-206 levels are typically quite low. However, under pathological conditions including myocardial infarction (MI), miR-206 is induced (Dong et al., 2009; Limana et al., 2011; Shan et al., 2009). Two MyHC isoforms are expressed in the heart: β-MyHC and the faster α-MyHC. One characteristic of multiple forms of heart disease is a shift towards a greater proportion of β-MyHC. To evaluate whether miR-206 induction is generalizable to pathologic conditions beyond MI, we treated wild-type male mice with the β-adrenergic receptor agonist isoproterenol. This chemically models pressure overload and is associated with β-MyHC induction. We saw a dose-responsive increase in miR-206 with a significant four-fold induction in 45 mg/kg-treated animals compared to vehicle controls (Fig. 6A).

Therefore, we proceeded to morphologically, functionally, and molecularly characterize hearts from 206KO animals. In males, we found a significant 11% increase in normalized left ventricle (LV) mass (Fig. 6B) with no change in female LVs (Supp. Fig. 7A). Similar to the soleus, we saw no dysregulation of other myomiRs, including miRs-133b, -1, -208a, or -208b (Supp. Fig. 6). Using M-mode echocardiography, we observed significant LV wall thinning and chamber dilation during systole in male 206KO mice compared to wild-type controls (Fig. 6C). Consistently, M-mode calculations revealed a 59% increase in male 206KO LV systolic volume

and an accompanying 17% decrease in ejection fraction and 25% decrease in percent fractional shortening, which were all statistically significant (Fig. 6D). Again, we saw no change in female LV dimensions or function (Supp. Fig. 7C, D).

We molecularly assessed the male 206KO LVs by qPCR-based analysis of a suite of mRNAs and miRNAs whose expression is frequently perturbed in numerous cardiac pathologies (Taegtmeyer et al., 2010; Van Rooij et al., 2006). These include RNAs encoding the atrial and B-type natriuretic peptides ANF and BNP, the skeletal muscle isoform of sarcomeric actin (Acta1), the calcium-handling factors Serca2a and Pln, the fetal cardiac transcription factors Gata4 and Nkx2.5, the Nfat target myocyte-enriched calcineurin-interacting protein (mCip1.4), the pro-fibrotic collagen 1 (Col1a1), and the anti-hypertrophic muscle cytokine myostatin (Mstn). Surprisingly, the only changes we observed were a 1.7-fold increase in Acta1 and a 1.6-fold decrease in Mstn, consistent with an increase in LV mass (Supp. Fig. 8A). We also observed no change in 10 miRNAs previously identified as part of a signature set of miRNAs whose expression levels respond to three different pathologic cardiac stimuli (Supp. Fig. 8B)(Van Rooij et al., 2006). However, when we measured MyHC mRNA levels, we saw a significant 1.4-fold induction of the faster cardiac isoform α-MyHC with a 1.3-fold downward trend in the slower β-MyHC (Fig. 6E). This suggests a shift towards a faster cardiac phenotype with pathologic functional consequences in the absence of miR-206 expression.

Discussion

We show that miR-206 is essential to enforce a slow muscle program in both skeletal muscle and the heart. In healthy skeletal muscle, miR-206 expression is strongly associated with the slow oxidative phenotype and is actually significantly higher in the female TA compared to male (Fig. 1A). This aligns with our previous observations that the female TA contains a greater

proportion of slow fibers in females and that females have a greater, but hormone-dependent, capacity for endurance exercise (Haines et al., 2012; Haizlip et al., 2015). There is likely to be a hormonal component to this expression pattern as aromatase null females express less miR-206 in the TA than wild-type females (Fig. 1B). Interestingly, estrogen can regulate miR-206 expression levels in breast cancer cells, further reinforcing this hormonal link (Adams et al., 2007). We did not see the same sex bias or response to aromatase deletion in expression of the miR-206 family member miR-1 nor in the genetically linked miR-133b, suggesting a specialized role for miR-206 in promoting the slower female phenotype.

The same miR-206 KO mouse studied here was shown to have delayed muscle regeneration after cardiotoxin injury, impaired satellite cell differentiation, and delayed neuromuscular reinnervation (Liu et al., 2012; Williams et al., 2009). Curiously, a separate knockout mouse that is lacking not only miR-206 but also miR-133b and a portion of the muscle regulatory long noncoding RNA linc-MD1 (including the sequence encoding a miR-133 sponge) displayed no overt phenotype at baseline, after acute muscle injury, or in the context of muscular dystrophy (Boettger et al., 2014). However, miR-206 and miR-133 family members have been shown to play opposing roles, where the former is pro-differentiation and anti-proliferative while the latter is pro-proliferative (Chen et al., 2006; Kim et al., 2006). Moreover, double knockout of miR-133 family members miR-133a-1 and miR-133a-2 (which, collectively, differ only at the terminal 3' position and so are presumed to target overlapping sets of transcripts) results in an increase in oxidative myofibers (Liu et al., 2011), also supporting opposing roles for miR-206 and the miR-133 family, potentially complicating interpretation of the miR-206/miR-133b double knockout mouse. Thus, to more fully elucidate the role of miR-206 in slow muscle, we phenotypically and molecularly characterized the soleus and left ventricles of miR-206 knockout

mice. In the soleus, we found a male-specific increase in muscle mass and an increase in the proportion of fast fiber types (Figs. 3,4). Supporting these observations, in Fig. 5 we show higher levels of the key fast muscle transcription factors Six1 and Eya1 (Grifone et al., 2004) as well as the fast-associated lncRNA linc-MYH, which is encoded at the fast MyHC locus, shares a Six1/Eya1-dependent enhancer with these MyHCs, and promotes fast-type gene expression (Sakakibara et al., 2014). The Six1 3' UTR harbors a predicted target site for another slow muscle-specific miRNA family, miR-208/499 (TargetScan.org). Transgenic miR-499 overexpression has been shown to convert all fast fibers in the mouse soleus to slow fibers (van Rooij et al., 2009). We did not observe differential expression of either miRNA in the miR-206 KO soleus, suggesting that miR-206 could be acting downstream of miR-499 and miR-208b in promoting the slow fiber program. We also saw increased Mef2c and myoglobin mRNA levels in the miR-206 KO soleus (Fig. 5), which may initially seem to contradict a fast-type phenotypic switch as expression of these genes is associated with an oxidative profile. However, a recent gene expression analysis of single soleus myofibers revealed that fast oxidative fibers (Types IIa and IIx) are characterized by a stronger mitochondrial and electron transport chain signature than Type I, which is consistent with our overall change in gene expression and fiber type profiles (Chemello et al., 2019).

miR-206 is well-studied in the context of the early stages of myogenesis, particularly in immortalized and primary myoblast cell culture models where it inhibits proliferation and promotes the transition to differentiation by targeting transcripts such as *Pola1*, *Pax7*, and *Pax3* (reviewed in (McCarthy, 2008; Mitchelson, 2015)). Although the targeting network through which it enforces a slow muscle phenotype is not yet clear, it notably targets the class II histone deacetylase (HDAC) *Hdac4* through translational inhibition (Williams et al., 2009; Winbanks et

al., 2011). Hdac4 inhibits slow muscle gene expression and, when knocked out in mice along with other class II HDACs, results in an increased proportion of Type I myofibers (Potthoff et al., 2007). This targeting relationship was established in the same miR-206 KO mice studied here when they were examined in the context of ALS (Williams et al., 2009).

In the heart, we also found that miR-206 promotes a slow phenotype. Although rodents express very little β-MyHC in the ventricles, these levels are not inconsequential and there are distinct regions where β-MyHC predominates (Krenz et al., 2007). In addition, α-MyHC:β-MyHC ratio is strictly regulated. Interestingly, β-MyHC expression is reportedly four-fold higher in the left ventricles of sexually mature female mice compared to males, and this difference is hormone-dependent (Patrizio et al., 2013). We have also previously reported that isolated female rat cardiomyocytes are slower to reach both peak shortening and relaxation (Trexler et al., 2017). These observations are consistent with our comparison of female and male TA muscle. As miR-206 levels are very low in the healthy ventricle, we could not reliably compare male and female expression levels. However, if miR-206 is also an enforcer of slow gene expression in the heart, we predicted that 1) in the absence of miR-206, the heart would shift towards a faster phenotype and 2) miR-206 expression would increase in pathologic conditions when the heart shifts towards a slower phenotype. Accordingly, we observed a significant increase in α-MyHC expression and a downward trend in β-MyHC expression in miR-206 KO LVs (Fig. 6E). Supporting the assertion that the small amount of β-MyHC that is expressed in the mouse heart is still critical for normal function, we observed ventricular dilation and systolic dysfunction in miR-206 KO mice (Figs. 6C,E). As in skeletal muscle, this is a male-specific phenomenon, the mechanistic basis for which is an intriguing area for future investigation. Interestingly, transgenic mice overexpressing miR-206 experience cardiac hypertrophy which, combined with our

knockout data, suggests the importance of maintaining miR-206 levels within a narrow range at baseline (Yang et al., 2015). However, miR-1 levels also increased in these transgenic miR-206 mice, and miR-1 overexpression in the heart is known to be detrimental (Zhao et al., 2005).

In support of our second prediction, we observed a dose-dependent increase in miR-206 expression in the left ventricles of mice treated with the β-adrenergic receptor agonist isoproterenol. Several reports have also noted increased miR-206 expression after MI in multiple animal models (Dong et al., 2009; Limana et al., 2011; Shan et al., 2009). Both MI and β-adrenergic stimulation are associated with an increase in β-MyHC expression at the expense of the faster α-MyHC (Harada et al., 1999). This may be a compensatory acute stress-adaptation mechanism as β-MyHC is a more efficient motor. We speculate that miR-206 KO mice would be less able to adapt to cardiac stress as they may not properly induce β-MyHC. Indeed, transgenic mice expressing a miR-206 sponge develop larger infarcts after ischemia/reperfusion injury than wild-type animals (Yang et al., 2015). As this miRNA sponge may also inhibit miR-1, which is the most abundant cardiac miRNA, it will be important to examine the response of miR-206 KO mice to cardiac injury in the future.

Collectively, our data indicate that miR-206 enforces slow muscle gene expression, which ultimately tunes both skeletal and cardiac muscle performance. Moreover, the consistent protective role of miR-206 under pathologic conditions in both tissues makes it an attractive target for RNA-based therapeutics.

Acknowledgments: We thank Dr. Eric Olson (UT-Southwestern) for generously providing the miR-206 KO mice. We also thank Amy Perry for performing echocardiography measurements, Darrian Bugge and Dr. Alberto Rossi for technical assistance, Drs. Emily Pugach and Christa

Trexler for valuable conversations and insight, and the University of Colorado Boulder BioFrontiers Advanced Light Microscopy Core facility for support with fluorescence microscopy.

Funding: This work was supported by NIH R016M29090 to L.A.L. K.K.B. was supported by NIH post-doctoral training grant 2T32HL007822-11A2 and AHA post-doctoral fellowship 13POST14410014, M.G.G. was supported by NIH pre-doctoral training grant 5T32GM007135-36, and BCH was supported by NIH Research Scientist Development Award K01AR055676.

References:

Adams BD, Furneaux H, White BA. 2007. The micro-ribonucleic acid (miRNA) miR-206 targets the human estrogen receptor-α (ERα) and represses ERα messenger RNA and protein expression in breast cancer cell lines. *Mol Endocrinol* **21**:1132–1147. doi:10.1210/me.2007-0022

Allen DL, Bandstra ER, Harrison BC, Thorng S, Stodieck LS, Kostenuik PJ, Morony S, Lacey DL, Hammond TG, Leinwand LL, Argraves WS, Bateman TA, Barth JL. 2009. Effects of spaceflight on murine skeletal muscle gene expression. *J Appl Physiol* **106**:582–595. doi:10.1152/japplphysiol.90780.2008

Allen DL, Harrison BC, Maass A, Bell ML, Byrnes WC, Leinwand LA. 2001. Cardiac and skeletal muscle adaptations to voluntary wheel running in the mouse. *J Appl Physiol* **90**:1900–1908.

Andersen P, Henriksson J. 1977. Training Induced Changes in the Subgroups of Human Type II Skeletal Muscle Fibres. *Acta Physiol Scand* **99**:123–125. doi:10.1111/j.1748-1716.1977.tb10361.x

Boettger T, Wüst S, Nolte H, Braun T. 2014. The miR-206/133b cluster is dispensable for development, survival and regeneration of skeletal muscle. *Skelet Muscle* **4**:23. doi:10.1186/s13395-014-0023-5

Caiozzo VJ, Baker MJ, Baldwin KM. 1998. Novel transitions in MHC isoforms: Separate and combined effects of thyroid hormone and mechanical unloading. *J Appl Physiol* **85**:2237–2248. doi:10.1152/jappl.1998.85.6.2237

Chemello F, Grespi F, Zulian A, Cancellara P, Hebert-Chatelain E, Martini P, Bean C, Alessio E, Buson L, Bazzega M, Armani A, Sandri M, Ferrazza R, Laveder P, Guella G, Reggiani C, Romualdi C, Bernardi P, Scorrano L, Cagnin S, Lanfranchi G. 2019. Transcriptomic Analysis of Single Isolated Myofibers Identifies miR-27a-3p and miR-142-3p as Regulators of Metabolism in Skeletal Muscle. *Cell Rep* **26**:3784–3797. doi:10.1016/j.celrep.2019.02.105

Chen JF, Mandel EM, Thomson JM, Wu Q, Callis TE, Hammond SM, Conlon FL, Wang DZ. 2006. The role of microRNA-1 and microRNA-133 in skeletal muscle proliferation and differentiation. *Nat Genet* **38**:228–233. doi:10.1038/ng1725

Cheung TH, Barthel KKB, Yin LK, Liu X. 2007. Identifying pattern-defined regulatory islands in mammalian genomes. *Proc Natl Acad Sci U S A* **104**:10116–10121. doi:10.1073/pnas.0704028104

Ciciliot S, Schiaffino S. 2010. Regeneration of Mammalian Skeletal Muscle: Basic Mechanisms and Clinical Implications. *Curr Pharm Des* **16**:906–914. doi:10.2174/138161210790883453

Dong S, Cheng Y, Yang J, Li J, Liu X, Wang X, Wang D, Krall TJ, Delphin ES, Zhang C. 2009. MicroRNA expression signature and the role of MicroRNA-21 in the early phase of acute

myocardial infarction. *J Biol Chem* **284**:29514–29525. doi:10.1074/jbc.M109.027896

Gokhin DS, Ward SR, Bremner SN, Lieber RL. 2008. Quantitative analysis of neonatal skeletal muscle functional improvement in the mouse. *J Exp Biol* **211**:837–843. doi:10.1242/jeb.014340

Grifone R, Laclef C, Spitz F, Lopez S, Demignon J, Guidotti J-E, Kawakami K, Xu P-X, Kelly R, Petrof BJ, Daegelen D, Concordet J-P, Maire P. 2004. Six1 and Eya1 Expression Can Reprogram Adult Muscle from the Slow-Twitch Phenotype into the Fast-Twitch Phenotype. *Mol Cell Biol* **24**:6253–6267. doi:10.1128/mcb.24.14.6253-6267.2004

Guess MG, Barthel KKB, Harrison BC, Leinwand LA. 2015. miR-30 family microRNAs regulate myogenic differentiation and provide negative feedback on the microRNA pathway. *PLoS One* **10**. doi:10.1371/journal.pone.0118229

Guess MG, Barthel KKB, Pugach EK, Leinwand LA. 2013. Measuring microRNA reporter activity in skeletal muscle using hydrodynamic limb vein injection of plasmid DNA combined with in vivo imaging. *Skelet Muscle* **3**:19. doi:10.1186/2044-5040-3-19

Haines CD, Harvey PA, Leinwand LA. 2012. Estrogens mediate cardiac hypertrophy in a stimulus-dependent manner. *Endocrinology* **153**:4480–4490. doi:10.1210/en.2012-1353

Haizlip KM, Harrison BC, Leinwand LA. 2015. Sex-based differences in skeletal muscle kinetics and fiber-type composition. *Physiology* **30**:30–39. doi:10.1152/physiol.00024.2014

Hamrick MW, Herberg S, Arounleut P, He HZ, Shiver A, Qi RQ, Zhou L, Isales CM, Mi QS. 2010. The adipokine leptin increases skeletal muscle mass and significantly alters skeletal muscle miRNA expression profile in aged mice. *Biochem Biophys Res Commun* **400**:379–

383. doi:10.1016/j.bbrc.2010.08.079

Harada K, Sugaya T, Murakami K, Yazaki Y, Komuro I. 1999. Angiotensin II type 1A receptor knockout mice display less left ventricular remodeling and improved survival after myocardial infarction. *Circulation* **100**:2093–2099. doi:10.1161/01.CIR.100.20.2093

Harrison BC, Allen DL, Girten B, Stodieck LS, Kostenuik PJ, Bateman TA, Morony S, Lacey D, Leinwand LA. 2003. Skeletal muscle adaptations to microgravity exposure in the mouse. *J Appl Physiol* **95**:2462–2470. doi:10.1152/japplphysiol.00603.2003

Izumo S, Lompré AM, Matsuoka R, Koren G, Schwartz K, Nadal-Ginard B, Mahdavi V. 1987. Myosin heavy chain messenger RNA and protein isoform transitions during cardiac hypertrophy. Interaction between hemodynamic and thyroid hormone-induced signals. *J Clin Invest* **79**:970–977. doi:10.1172/JCI112908

Janssen I, Heymsfield SB, Wang Z, Ross R. 2000. Skeletal muscle mass and distribution in 468 men and women aged 18-88 yr. *J Appl Physiol* **89**:81–88.

Kim HK, Lee YS, Sivaprasad U, Malhotra A, Dutta A. 2006. Muscle-specific microRNA miR-206 promotes muscle differentiation. *J Cell Biol* **174**:677–687. doi:10.1083/jcb.200603008

Kim JY, Park YK, Lee KP, Lee SM, Kang TW, Kim HJ, Dho SH, Kim SY, Kwon KS. 2014. Genome-wide profiling of the microRNA-mRNA regulatory network in skeletal muscle with aging. *Aging (Albany NY)* **6**:524–544. doi:10.18632/aging.100677

Krenz M, Sadayappan S, Osinska HE, Henry JA, Beck S, Warshaw DM, Robbins J. 2007. Distribution and structure-function relationship of myosin heavy chain isoforms in the adult mouse heart. *J Biol Chem* **282**:24057–24064. doi:10.1074/jbc.M704574200

Limana F, Esposito G, D'Arcangelo D, Di Carlo A, Romani S, Melillo G, Mangoni A, Bertolami C, Pompilio G, Germani A, Capogrossi MC. 2011. HMGB1 attenuates cardiac remodelling in the failing heart via enhanced cardiac regeneration and miR-206-mediated inhibition of TIMP-3. *PLoS One* **6**:e19845. doi:10.1371/journal.pone.0019845

Liu N, Bezprozvannaya S, Shelton JM, Frisard MI, Hulver MW, McMillan RP, Wu Y, Voelker KA, Grange RW, Richardson JA, Bassel-Duby R, Olson EN. 2011. Mice lacking microRNA 133a develop dynamin 2-dependent centronuclear myopathy. *J Clin Invest* **121**:3258–3268. doi:10.1172/JCI46267

Liu N, Williams AH, Maxeiner JM, Bezprozvannaya S, Shelton JM, Richardson JA, Bassel-Duby R, Olson EN. 2012. microRNA-206 promotes skeletal muscle regeneration and delays progression of Duchenne muscular dystrophy in mice. *J Clin Invest* **122**:2054–2065. doi:10.1172/JCI62656

Ma G, Wang Y, Li Y, Cui L, Zhao Y, Zhao B, Li K. 2015. MiR-206, a key modulator of skeletal muscle development and disease. *Int J Biol Sci* **11**:345–352. doi:10.7150/ijbs.10921

McCarthy JJ. 2008. MicroRNA-206: The skeletal muscle-specific myomiR. *Biochim Biophys Acta - Gene Regul Mech* **1779**:682–691. doi:10.1016/j.bbagrm.2008.03.001

McCarthy JJ, Fox AM, Tsika GL, Gao L, Tsika RW. 1997. β-MHC transgene expression in suspended and mechanically overloaded/suspended soleus muscle of transgenic mice. *Am J Physiol - Regul Integr Comp Physiol* **272**:R1552-61.

Mitchelson KR. 2015. Roles of the canonical myomiRs miR-1, -133 and -206 in cell development and disease. *World J Biol Chem* **6**:162–208. doi:10.4331/wjbc.v6.i3.162

Miyata S, Minobe W, Bristow MR, Leinwand LA. 2000. Myosin Heavy Chain Isoform Expression in the Failing and Nonfailing Human Heart. *Circ Res* **86**:386–390. doi:10.1161/01.RES.86.4.386

Nakao K, Minobe W, Roden R, Bristow MR, Leinwand LA. 1997. Myosin heavy chain gene expression in human heart failure. *J Clin Invest* **100**:2362–2370. doi:10.1172/JCI119776

O'Rourke JR, Georges SA, Seay HR, Tapscott SJ, McManus MT, Goldhamer DJ, Swanson MS, Harfe BD. 2007. Essential role for Dicer during skeletal muscle development. *Dev Biol* **311**:359–368. doi:10.1016/j.ydbio.2007.08.032

Patrizio M, Musumeci M, Piccone A, Raggi C, Mattei E, Marano G. 2013. Hormonal regulation of β-myosin heavy chain expression in the mouse left ventricle. *J Endocrinol* **216**:287–296. doi:10.1530/JOE-12-0201

Potthoff MJ, Wu H, Arnold MA, Shelton JM, Backs J, McAnally J, Richardson JA, Bassel-Duby R, Olson EN. 2007. Histone deacetylase degradation and MEF2 activation promote the formation of slow-twitch myofibers. *J Clin Invest* **117**:2459–2467. doi:10.1172/JCI31960

Rao PK, Kumar RM, Farkhondeh M, Baskerville S, Lodish HF. 2006. Myogenic factors that regulate expression of muscle-specific microRNAs. *Proc Natl Acad Sci* **103**:8721–8726. doi:10.1073/pnas.0602831103

Resnicow DI, Deacon JC, Warrick HM, Spudich JA, Leinwand LA. 2010. Functional diversity among a family of human skeletal muscle myosin motors. *Proc Natl Acad Sci U S A* **107**:1053–1058. doi:10.1073/pnas.0913527107

Ross A, Leveritt M. 2001. Long-term metabolic and skeletal muscle adaptations to short-sprint

training: Implications for sprint training and tapering. *Sport Med* **31**:1063–1082. doi:10.2165/00007256-200131150-00003

Sakakibara I, Santolini M, Ferry A, Hakim V, Pascal M. 2014. Six Homeoproteins and a Iinc-RNA at the Fast MYH Locus Lock Fast Myofiber Terminal Phenotype. *PLoS Genet* **10**:e1004386. doi:10.1371/journal.pgen.1004386

Shan ZX, Lin QX, Fu YH, Deng CY, Zhou ZL, Zhu JN, Liu XY, Zhang YY, Li Y, Lin SG, Yu XY. 2009. Upregulated expression of miR-1/miR-206 in a rat model of myocardial infarction. *Biochem Biophys Res Commun* **381**:597–601. doi:10.1016/j.bbrc.2009.02.097

Sweetman D, Goljanek K, Rathjen T, Oustanina S, Braun T, Dalmay T, Münsterberg A. 2008. Specific requirements of MRFs for the expression of muscle specific microRNAs, miR-1, miR-206 and miR-133. *Dev Biol* **321**:491–499. doi:10.1016/j.ydbio.2008.06.019

Taegtmeyer H, Sen S, Vela D. 2010. Return to the fetal gene program: A suggested metabolic link to gene expression in the heart. *Ann N Y Acad Sci* **1188**:191–198. doi:10.1111/j.1749-6632.2009.05100.x

Trexler CL, Odell AT, Jeong MY, Dowell RD, Leinwand LA. 2017. Transcriptome and Functional Profile of Cardiac Myocytes Is Influenced by Biological Sex. *Circ Cardiovasc Genet* **10**:pii: e001770. doi:10.1161/CIRCGENETICS.117.001770

van Rooij E, Quiat D, Johnson BA, Sutherland LB, Qi X, Richardson JA, Kelm RJ, Olson EN. 2009. A family of microRNAs encoded by myosin genes governs myosin expression and muscle performance. *Dev Cell* **17**:662–73. doi:10.1016/j.devcel.2009.10.013

Van Rooij E, Sutherland LB, Liu N, Williams AH, McAnally J, Gerard RD, Richardson JA,

Olson EN. 2006. A signature pattern of stress-responsive microRNAs that can evoke cardiac hypertrophy and heart failure. *Proc Natl Acad Sci U S A* **103**:18255–18260. doi:10.1073/pnas.0608791103

Webster C, Silberstein L, Hays AP, Blau HM. 1988. Fast muscle fibers are preferentially affected in Duchenne muscular dystrophy. *Cell* **52**:503–513. doi:10.1016/0092-8674(88)90463-1

Williams AH, Valdez G, Moresi V, Qi X, McAnally J, Elliott JL, Bassel-Duby R, Sanes JR, Olson EN. 2009. MicroRNA-206 delays ALS progression and promotes regeneration of neuromuscular synapses in mice. *Science (80-)* **326**:1549–1554. doi:10.1126/science.1181046

Winbanks CE, Wang B, Beyer C, Koh P, White L, Kantharidis P, Gregorevic P. 2011. TGF-β regulates miR-206 and miR-29 to control myogenic differentiation through regulation of HDAC4. *J Biol Chem*. doi:10.1074/jbc.M110.192625

Yang Y, Del Re DP, Nakano N, Sciarretta S, Zhai P, Park J, Sayed D, Shirakabe A, Matsushima S, Park Y, Tian B, Abdellatif M, Sadoshima J. 2015. MIR-206 Mediates YAP-Induced Cardiac Hypertrophy and Survival. *Circ Res* **117**:891–904. doi:10.1161/CIRCRESAHA.115.306624

Yuasa K, Ando M, Nakamura A, Takeda S, Hagiwara Y, Hijikata T. 2008. MicroRNA-206 Is Highly Expressed in Newly Formed Muscle Fibers: Implications Regarding Potential for Muscle Regeneration and Maturation in Muscular Dystrophy. *Cell Struct Funct*. doi:10.1247/csf.08022

Yutzey KE, Konieczny SF. 1992. Different E-box regulatory sequences are functionally distinct

when placed within the context of the troponin I enhancer. *Nucleic Acids Res* **20**:5105–5113. doi:10.1093/nar/20.19.5105

Zhao Y, Samal E, Srivastava D. 2005. Serum response factor regulates a muscle-specific microRNA that targets Hand2 during cardiogenesis. *Nature* **436**:214–220. doi:10.1038/nature03817

Figure Legends:

Figure 1. miR-206 expression is highest in slow twitch muscle and is up-regulated with endurance exercise. (A) miR-206 levels are highest in slow muscles in both sexes (left panel) but higher in female (F) compared to male (M) fast TA (right panel). We assessed miR-206 expression by qPCR in tibialis anterior (TA), gastrocnemius and plantaris (GP), and soleus (SOL) from both male and female mice. Expression relative to male TA is presented. N are as follows: 8 M TA, 8 F TA, 9 M GP, 8 F GP, 10 M SOL, 8 F SOL; *** = $p \leq 0.001$ SOL vs. TA or vs. GP within each sex, * = $p \leq 0.05$ F vs. M TA **(B)** miR-206 expression is lower in TAs from aromatase null compared to WT female mice. We measured miR-206 levels as in (A). Fold change (FC) relative to WT F TA is presented. N was 5 in both groups. ** = $p \leq 0.01$ **(C)** In male mice, miR-206 expression increases by 3 days after initiating voluntary cage wheel running and then returns to baseline but it does not change with muscle unloading by hindlimb suspension (HS). We measured miR-206 as in (A). Fold change relative to normal cage activity controls (represented by the dashed line at y = 1) is presented. N are as follows: 6 control, 5 3d run, 3 7d run, 3 14d run, 6 3d HS, 3 7d HS, 3 14d HS; ** = $p \leq 0.01$ 3d run vs control.

Figure 2. miR-206 is transcriptionally up-regulated in pathologic conditions that shift fast muscles to a slower phenotype. (A) miR-206 levels are higher in dystrophic (*mdx4cv*) fast muscles (TA and GP) compared to WT mice but not different in slow soleus (SOL). We measured miR-206 levels as in Figure 1. N was 5 for all WT muscles and 4 for all *mdx4cv* muscles. *** = $p \leq 0.001$ *mdx4cv* vs WT for TA and GP. **(B)** miR-206 levels are higher in *vastus lateralis* (VL) muscle from human DMD patients compared to healthy controls. We measured miR-206 levels as in Figure 1 but normalized to U6 RNA levels. N was 5 for both groups. ** = $p \leq 0.01$ DMD vs WT **(C and D)** Mature miR-206 (C) and pri-miR-206 (D) levels increase in regenerating TA after $BaCl_2$ injury at the indicated days post-injury (dpi). Pri-miR-206 levels peak before (3dpi) mature miR-206 levels (14dpi). We measured mature miR-206 levels as in Figure 1. We measured pri-miR-206 by qPCR; expression levels relative to the uninjured (PBS-injected) contralateral control TA are presented. Control levels are represented as a dashed line at y = 1. Ns for 3 dpi, 7 dpi, and 14 dpi were 5, 3, and 3, respectively. *** = $p \leq 0.001$ vs. control. **(E)** A luciferase reporter gene driven by the miR-206 enhancer is up-regulated *in vivo* during muscle regeneration. We injected the miR-206 enhancer reporter construct or the minTATA negative control reporter into the hindlimb of mice through the great saphenous vein under high pressure. We subsequently injured the gastrocnemius with $BaCl_2$ ("injury") or injected it with PBS as a control ("sham"). We determined longitudinal changes in reporter gene activity in live mice by injecting luciferin at days 1, 3, 7, and 28 after injury and measuring luciferase activity. Representative images of miR-206 reporter mice are shown (sham mouse on the top, injured mouse on the bottom). We performed region of interest analysis and quantified bioluminescence signal, expressed as photons/second/cm2/steradian (p/sec/cm2/sr). Signal intensity was false colored according to the color bar below. Average signal intensities are

plotted to the right. Asterisk denotes statistical significance vs. control group injected with the same plasmid: * = $p \leq 0.05$.

Figure 3. miR-206 KO increases male soleus mass and myofiber cross-sectional area. (A) Soleus (SOL) mass is higher in miR-206 KO (206KO) male mice compared to WT controls. Muscle mass normalized to tibia length (TL) is presented. N are as follows: 7 WT, 6 206KO; ** = $p \leq 0.01$ **(B)** Representative laminin-stained soleus cross-sections from WT (left) and 206KO (right) male mice. Scale bar denotes 100 μm. **(C)** There is a shift towards larger cross-sectional area (CSA) in myofibers from 206KO compared to WT male mice. We measured CSA across entire soleus cross-sections from 3 mice of each genotype and calculated the proportion of myofibers in 100 μm^2 bins. Only 206KO mice had any myofibers larger than 1300 μm^2.

Figure 4. The proportion of slow fibers decreases while fast fibers increase in miR-206 KO soleus. (A) Representative MyHC-stained soleus cross-sections from WT (left) and 206KO (right) male mice. Type I (β-MyHC) fibers are purple, Type IIa are red, and Type IIx are green. Nuclei are revealed by DAPI staining (blue). Scale bar denotes 100 μm. **(B)** Quantification of proportions Type I, IIa, and IIx fibers across entire soleus cross-sections from 6 WT and 4 206KO male mice (left panel) and the percent change in each fiber type (right panel; 206KO vs WT). * = $p \leq 0.05$, ** = $p \leq 0.01$ 206KO vs WT. **(C)** Fast MyHC mRNA levels increase in male 206KO soleus compared to WT. We measured mRNA levels of β-MyHC, MyHC IIa, and MyHC IIx with qPCR as in Fig. 2D and normalized to actin (Acta1). WT levels are represented as a dashed line at y = 1. N was 4-6 for each group. * = $p \leq 0.05$, ** = $p \leq 0.01$ 206KO vs WT.

Figure 5. The gene expression signature of the miR-206 KO soleus shifts towards fast oxidative. We measured mRNA levels of genes from diverse functional categories in the soleus

by qPCR. WT levels are represented as a dashed line at y = 1. N was 5 for each group. * = $p \leq 0.05$, ** = $p \leq 0.01$ 206KO vs WT.

Figure 6. miR-206 is associated with slow MyHC expression in the LV and knockout results in cardiac dilation and systolic dysfunction. (A) A dose-dependent increase in miR-206 levels in the LVs of male WT mice treated 1 week with the indicated amounts of isoproterenol. We measured miR-206 expression as in Fig. 1. N was 6 for vehicle control and 8 for both 30 mg/kg and 45 mg/kg. * = $p \leq 0.05$ vs. vehicle. **(B)** Left ventricle (LV) mass normalized to tibia length (TL) is higher in 206KO males compared to WT. N was 7 for WT and 6 for 206KO. * = $p \leq 0.05$ vs. WT. **(C and D)** M-mode echocardiographic measurements (C) and calculations (D) indicate LV dilation and systolic dysfunction in male 206KO mice. We measured LV anterior wall (LVAW) thinning, increased LV interior diameter (LVID), and increased LV volume (LV Vol). Both ejection fraction (EF) and fractional shortening (FS) decreased. N was 4 for WT and 5 for 206KO. * = $p \leq 0.05$, ** = $p \leq 0.01$ 206KO vs. WT. **(E)** mRNA corresponding to the faster cardiac α-MyHC increases while the slower β-MyHC decreases in male 206KO LV compared to WT. We measured MyHC mRNA levels with qPCR as in Fig. 2D. WT levels are represented as a dashed line at y = 1. N was 6 for each group. * = $p \leq 0.05$ 206KO vs WT.

Supplemental Figure 1. myomiR expression in male, female, and female ArKO muscles. (A) Expression of miR-1, miR-133b, and miR-133a is not different between male and female mice in the TA. N was 7 for males (M) and 8 for females (F). **(B)** In the gastrocnemius and plantaris (GP) and in the soleus (SOL), miR-206 expression is not different between WT and aromatase KO (ArKO) females. N was 5 for both groups. **(C)** Expression of miR-1, miR-133b, and miR-133a is not different between WT and ArKO female mice in the TA. N was 5 for both groups. In all panels, we measured miRNA levels by qPCR as in Fig. 1.

Supplemental Figure 2. *In vivo* imaging of basal promoter-driven reporter gene expression. Reporter gene activity imaging of minTATA negative control reporter as described and quantified in Fig. 2E. Signal intensity was false colored according to the color bar below.

Supplemental Figure 3. The miR-206 transcriptional enhancer is dependent on conserved, muscle-specific E-boxes. (A) A 207-bp region approximately 1 kb upstream of the miR-206 locus (screenshot from Genome Browser (genome.ucsc.edu)) contains spikes in conservation (blue histogram) corresponding to E-box consensus sites. The line drawing below this screenshot indicates the location of the E-boxes conforming to the consensus sequence CANNTG, with E-boxes conserved in human, mouse, and rat shown in red and those not conserved in human shown in cyan. The complete mouse sequence cloned for reporter gene analysis is also shown with E-boxes similarly color-coded. **(B)** Activity of a firefly luciferase reporter gene with the 200-bp genomic region cloned upstream of a minimal TATA-box-containing promoter increases during differentiation of C2C12 cells. We transfected C2C12 cells with the constructs indicated on the x-axis. We induced differentiation by serum withdrawal 24 hours post-transfection and measured reporter activity at Day 0 (proliferating myoblasts), Day 1, and Day 4 after differentiation initiation. We normalized firefly luciferase activity to renilla luciferase activity from the same lysates. MyoG serves as a positive control and has the myogenin enhancer driving firefly luciferase. We performed all experiments in triplicate. Asterisks denote $p \leq 0.01$ vs. Day 0, double daggers denote $p \leq 0.01$ vs. Day 1. **(C)** The miR-206 200-bp reporter responds to expression of muscle regulatory factors (MRFs) in mouse 10T1/2 fibroblasts. We transfected 10T1/2 cells with the reporters indicated on the x-axis (described in (B)) and either empty vector control or overexpression constructs for Flag-tagged MRFs. MyoG and miR-206 200-bp both respond to all 4 MRFs, but the strength of activation in the presence of the various MRFs differs

between the reporters. Experiments were performed in triplicate. Asterisks denote statistical significance vs. Empty Vector: ** = $p \leq 0.01$; *** = $p \leq 0.001$. **(D)** We analyzed E-boxes from the mouse 200-bp region (numbered from the 5' to the 3' end of the cloned region as cartooned in A) and the orthologous human region for conformation to the longer muscle-specific E-box consensus sequence described by Buskin & Hauschka. The consensus is above the table with the core E-box in red text. The scoring rubric is 0 points for divergence, 0.5 points for a degenerate sequence match, and 1 point for an invariant sequence match (8 = highest possible score). Asterisks indicate divergence from the muscle consensus sequence. Ø indicates that there is no orthologous human CANNTG sequence. **(E)** Only conserved E-boxes contribute to transcriptional activation from the miR-206 enhancer. We mutated E-boxes in the WT miR-206 200-bp construct from CANNTG to CANNTA. We mutated conserved E-boxes 1, 2, and 5 individually while we mutated unconserved E-boxes 3 and 4 together in one construct. Finally, we mutated all 5 E-boxes in the construct named E-boxless. We transfected C2C12 cells with each mutant construct as well as the WT and allowed them to differentiate for one day. We normalized firefly luciferase activity to control renilla luciferase activity and analyzed D1 vs. D0 for statistical significance: *** = $p \leq 0.001$. We performed all experiments in triplicate.

Supplemental Figure 4. Muscle masses in male and female miR-206 KO vs WT mice. (A) Muscle mass (gastrocnemius and plantaris (GP), tibialis anterior (TA)) comparison between 206KO and WT male mice. We normalized muscle masses to tibia length (TL). N are as follows: 7 WT GP, 6 206KO GP, 7 WT TA, 5 206KO TA. **(B)** Muscle mass (soleus (SOL), gastrocnemius and plantaris (GP), tibialis anterior (TA)) comparison between 206KO and WT female mice. We normalized muscle masses to tibia length (TL). N is 5 for WT, 3 for 206KO.

Supplemental Figure 5. myomiR and linc-MD1 RNA expression in miR-206 KO vs WT soleus. (A) We verified that miR-206 is undetectable in the 206KO male soleus. There is also no compensatory change in miR-1 or miR-133b expression. We measured miRNA expression as in Fig. 1. N was 6 for both genotypes. **(B)** linc-MD1 expression does not change in 206KO soleus compared to WT. We measured RNA expression as in Fig. 5. N was 7 for WT, 6 for 206KO.

Supplemental Figure 6. myomiR expression in miR-206 KO vs WT LVs. There is no change in miRs -133b, -1, -208a, or -208b in the male 206KO left ventricle (LV) compared to WT. We measured miRNA expression as in Fig. 1. N was 7 for WT, 6 for 206KO.

Supplemental Figure 7. LV mass and M-mode echocardiography measurements in miR-206 KO vs WT female mice. (A) Left ventricle (LV) mass normalized to tibia length (TL) is not different between 206KO females and WT. N was 5 for WT and 3 for 206KO. **(B)** Heart rate was the same in all groups of animals. N was 4 for WT male (M), 5 for 206KO M, 5 for WT female (F), and 4 for 206KO F. **(C and D)** M-mode echocardiographic measurements (C) and calculations (D) revealed no changes in LV dimensions or function in female 206KO mice. LV anterior wall = LVAW, LV interior diameter = LVID, LV volume = LV Vol, ejection fraction = EF, and fractional shortening = FS. N was 5 for WT and 4 for 206KO.

Supplemental Figure 8. Expression of mRNA and miRNA cardiac stress markers in miR-206 KO vs WT LVs. (A) We measured mRNA levels corresponding to the indicated genes as in Fig. 6 and compared male 206KO LV to WT. Acta1 was significantly up-regulated while Mstn was significantly down-regulated. WT levels are represented as a dashed line at y = 1. N was 7 for WT and 6 for 206KO. * = $p \leq 0.05$ 206KO vs WT. **(B)** We measured miRNA levels corresponding to the indicated genes as in Fig. 1 and compared male 206KO LV to WT. WT levels are represented as a dashed line at y = 1. N was 7 for WT and 6 for 206KO.

Supplemental Table 1. Primer sequences. Primers for cloning the miR-206 enhancer, mutagenizing the E-boxes in the miR-206 enhancer, qPCR analysis, and genotyping mice are presented 5' → 3'.

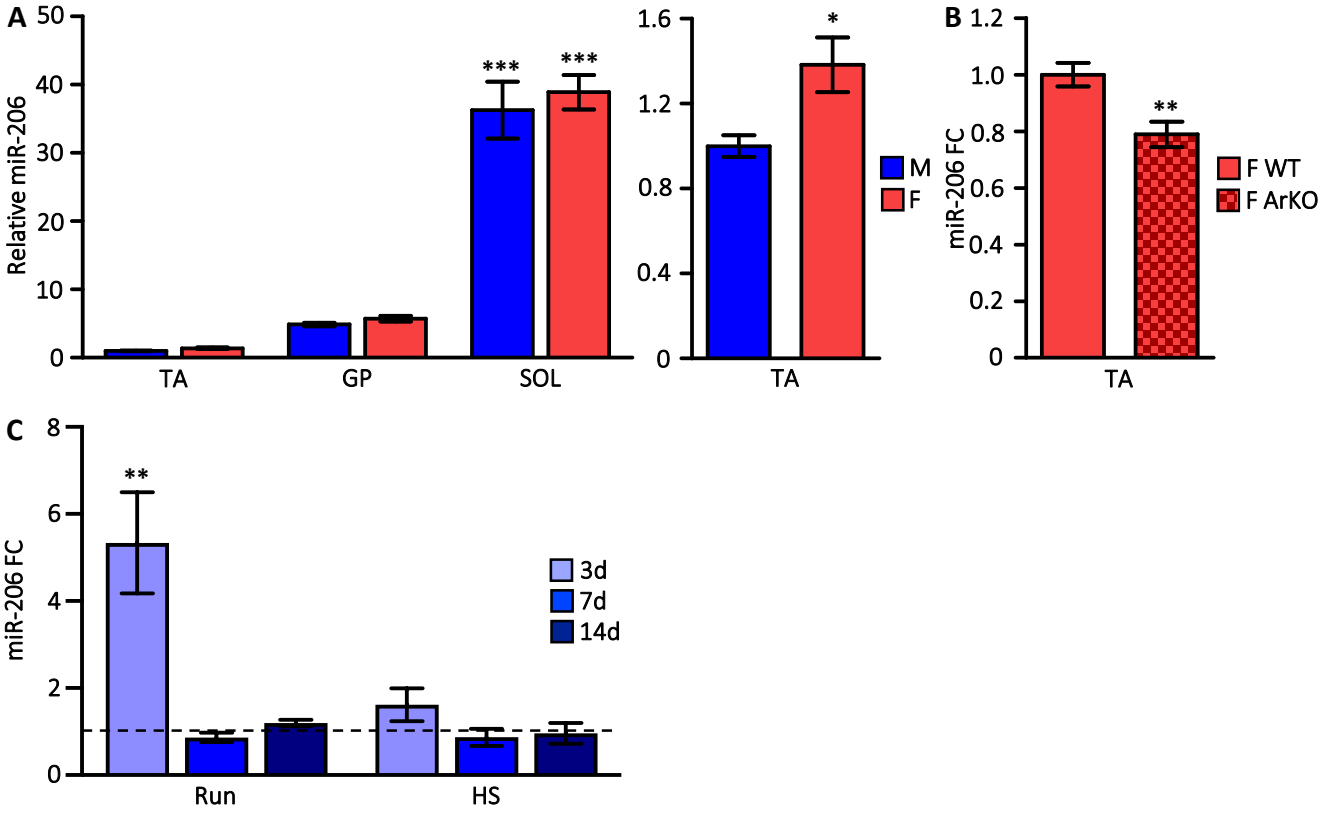
A
Relative miR-206
50
40
30
20
10
0
***
***
TA
GP
SOL
1.6
1.2
0.8
0.4
0
*
TA
M
F
B
miR-206 FC
1.2
1.0
0.8
0.6
0.4
0.2
0
**
TA
F WT
F ArKO
C
miR-206 FC
8
6
4
2
0
**
Run
HS
3d
7d
14d

Figure 1

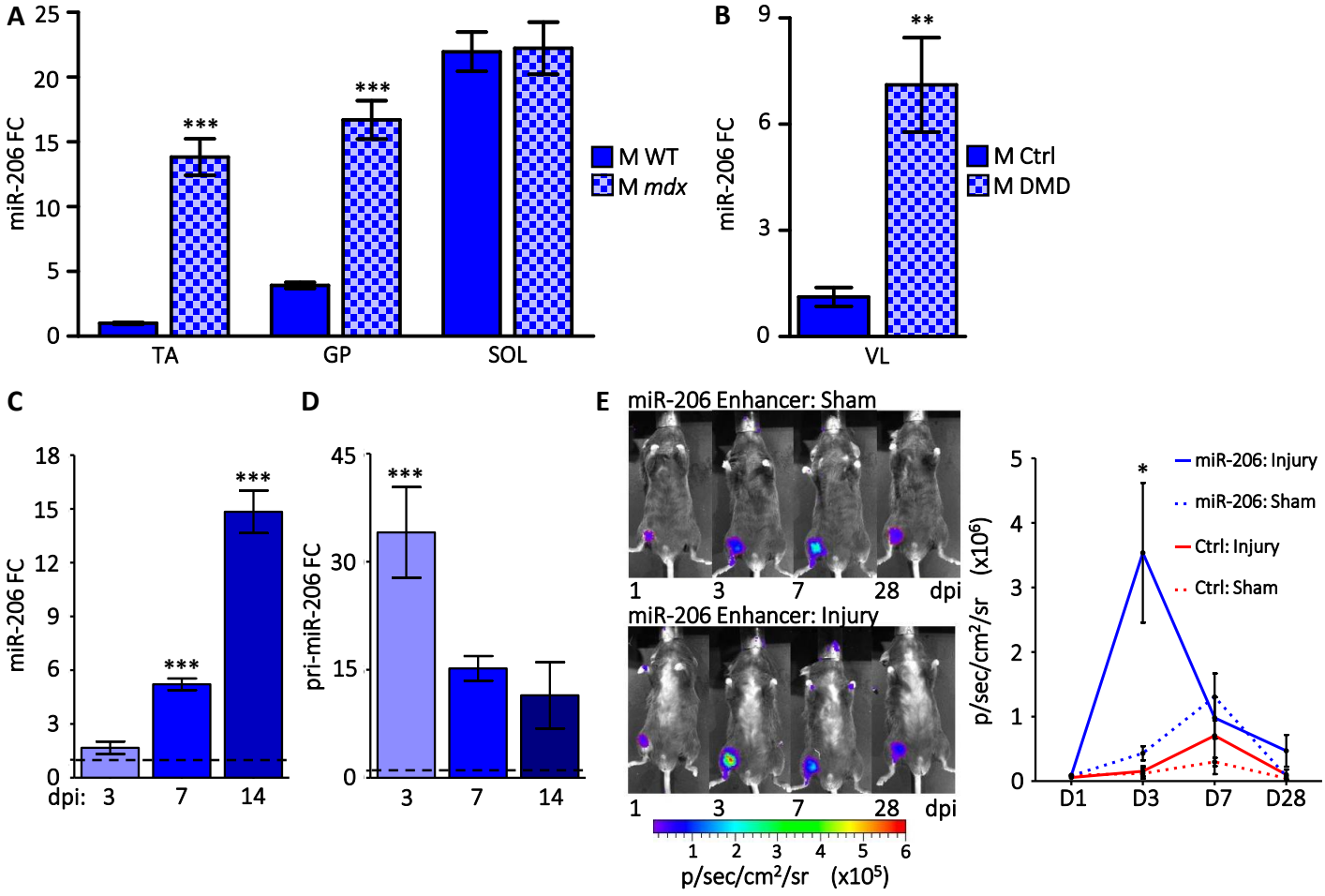
A
miR-206 FC
25
20
15
10
5
0
***
***
TA
GP
SOL
M WT
M mdx
B
miR-206 FC
9
6
3
0
**
VL
M Ctrl
M DMD
C
miR-206 FC
18
15
12
9
6
3
0
***
***
dpi: 3
7
14
D
pri-miR-206 FC
45
30
15
0
***
3
7
14
E
miR-206 Enhancer: Sham
1
3
7
28
dpi
miR-206 Enhancer: Injury
1
3
7
28
dpi
1
2
3
4
5
6
p/sec/cm²/sr (x10⁵)
p/sec/cm²/sr (x10⁶)
5
4
3
2
1
0
*
miR-206: Injury
miR-206: Sham
Ctrl: Injury
Ctrl: Sham
D1
D3
D7
D28

Figure 2

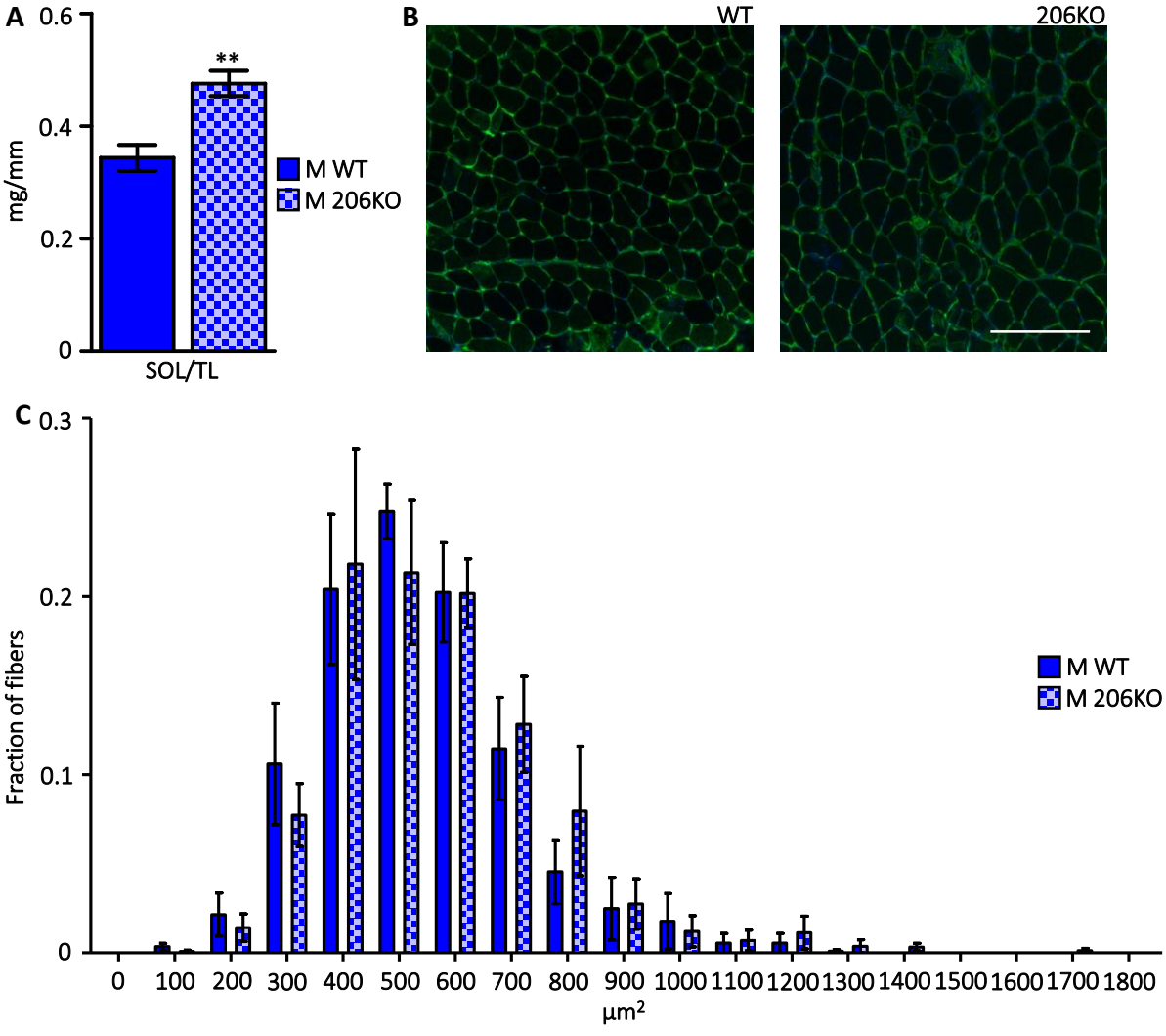
A
0.6
0.4
0.2
0
mg/mm
**
M WT
M 206KO
SOL/TL
B
WT
206KO
C
0.3
0.2
0.1
0
Fraction of fibers
M WT
M 206KO
0
100
200
300
400
500
600
700
800
900
1000
1100
1200
1300
1400
1500
1600
1700
1800
µm²

Figure 3

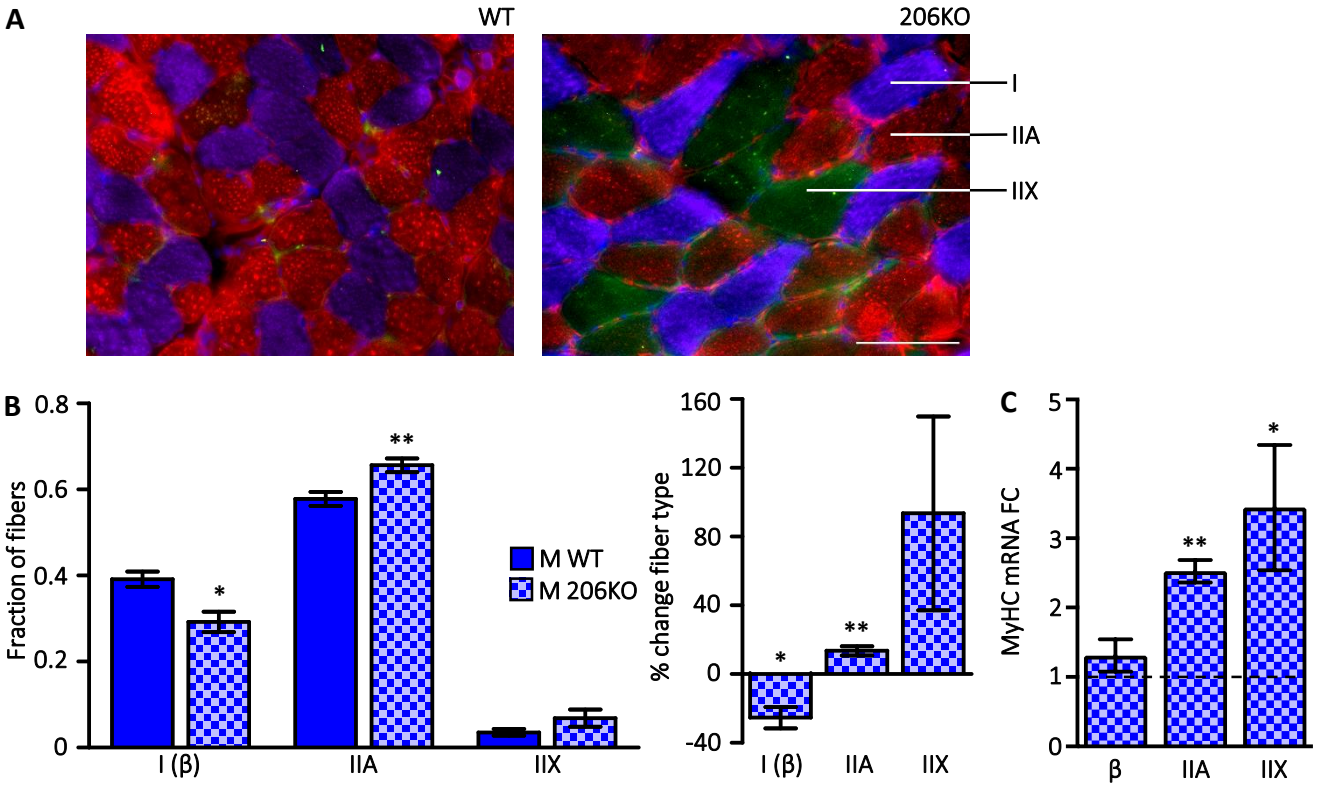
A
WT
206KO
I
IIA
IIX
B
Fraction of fibers
0.8
0.6
0.4
0.2
0
*
**
M WT
M 206KO
I (β)
IIA
IIX
% change fiber type
160
120
80
40
0
-40
*
**
I (β)
IIA
IIX
C
MyHC mRNA FC
5
4
3
2
1
0
**
*
β
IIA
IIX

Figure 4

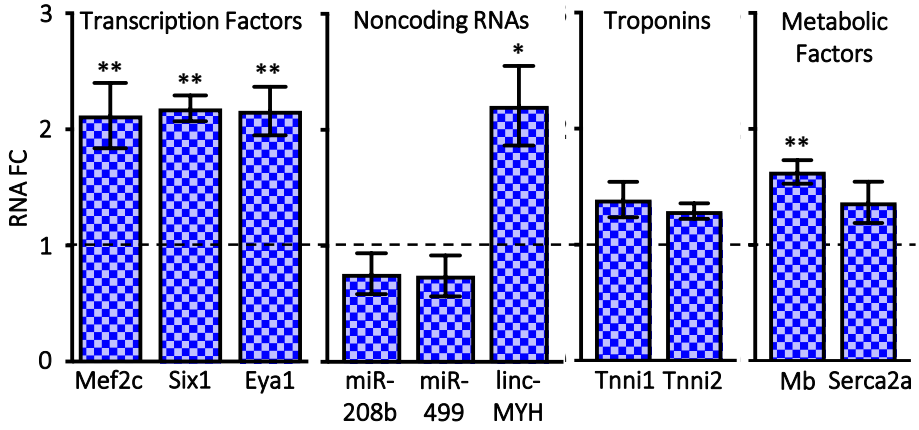
Transcription Factors
Noncoding RNAs
Troponins
Metabolic Factors
RNA FC
3
2
1
0
**
**
**
*
**
Mef2c
Six1
Eya1
miR-208b
miR-499
linc-MYH
Tnni1
Tnni2
Mb
Serca2a

Figure 5

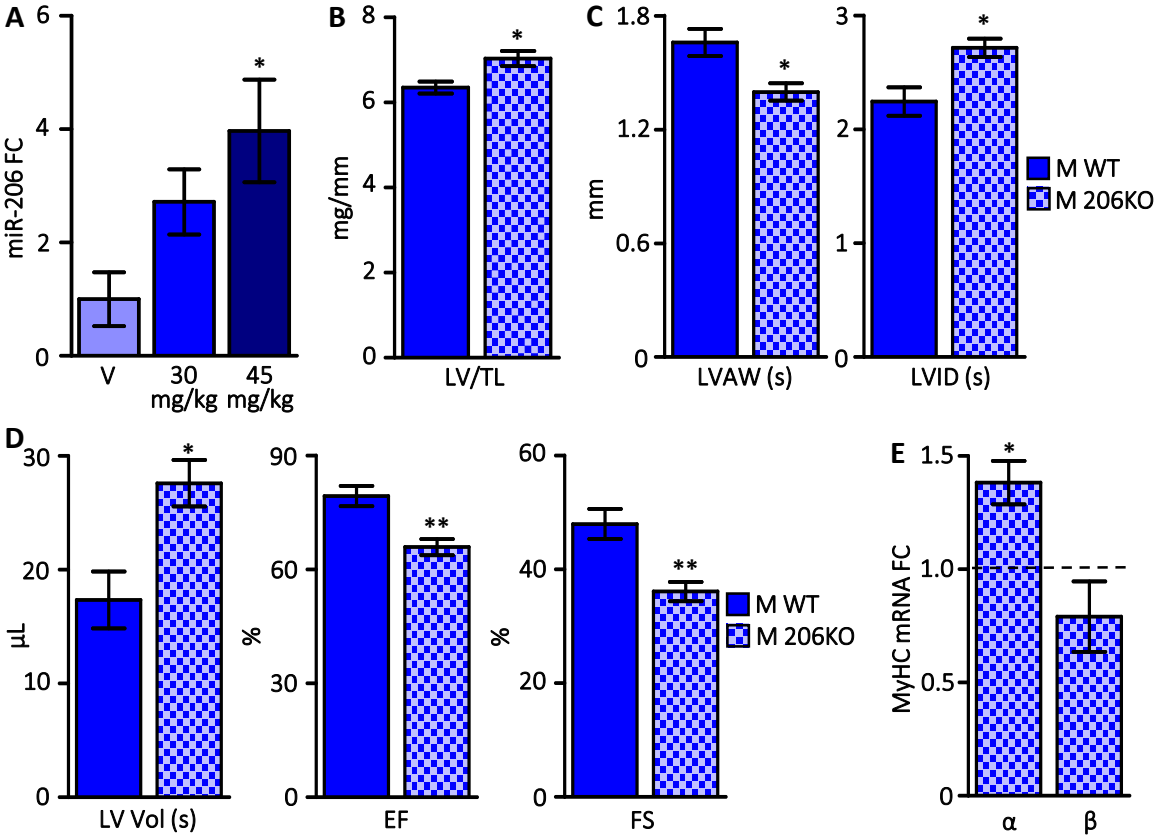
A
miR-206 FC
V
30 mg/kg
45 mg/kg
B
mg/mm
LV/TL
C
mm
LVAW (s)
LVID (s)
M WT
M 206KO
D
µL
LV Vol (s)
%
EF
%
FS
E
MyHC mRNA FC
α
β

Figure 6